ELSEVIER

Chemical Geology 183 (2002) 25–41

CHEMICAL GEOLOGY
INCLUDING
ISOTOPE GEOSCIENCE

www.elsevier.com/locate/chemgeo

Modeling the major-element evolution of olivine-hosted melt inclusions

Glenn A. Gaetani [a,b,*], E. Bruce Watson [a]

[a] Department of Earth and Environmental Sciences, Rensselaer Polytechnic Institute, Troy, NY 12180, USA
[b] Department of Geology and Geophysics, Woods Hole Oceanographic Institution, Woods Hole, MA 02543, USA

Received 8 September 2000; received in revised form 13 June 2001

Abstract

This paper presents a detailed description of an approach for modeling the major element evolution of olivine-hosted melt inclusions. Numerical simulations constrained by experimental data on olivine/melt equilibrium and interdiffusion rates of Fe and Mg in olivine quantify the post-entrapment processes (crystallization, dissolution, Fe–Mg exchange with the host) that influence the major element compositions of included melts. Equilibrium at the olivine/melt interface is described by expressions for FeO and MgO partitioning calibrated using olivine–liquid pairs from the literature spanning temperatures of 1064 to 1950 °C and pressures of 1 bar to 70 kbar. The liquidus temperature and equilibrium olivine composition are calculated simultaneously for melt of a given composition using the partitioning expressions and olivine stoichiometry. Diffusion in the host olivine is modeled by the explicit finite-difference method. The main inputs for a simulation are the initial composition and size of the melt inclusion, the size of the host olivine, and the desired cooling path expressed as a constant cooling rate. The rate of olivine crystallization (dF/dT) within an inclusion is dynamically adjusted with each time step so that the observed Fe–Mg exchange coefficient (K_D^{Fe-Mg}) at the inclusion/host interface matches the equilibrium value predicted by the partitioning equations. Application of the approach to model the major element evolution of an inclusion formed within the melting regime beneath an oceanic spreading center indicates that the composition of the included melt is significantly modified during transport to the surface along the mantle geotherm. Further, the compositional path followed by the included melt is dependent upon the capacity of the host olivine to maintain the inclusion at the pressure of entrapment. © 2002 Published by Elsevier Science B.V.

Keywords: Olivine; Melt; Fe–Mg exchange

1. Introduction

Silicate melts included in olivine and plagioclase crystals preserve a range of compositional and isotopic variability not found in erupted lavas, providing a unique and invaluable geochemical tool for studying the processes of melt generation and migration in the upper mantle of the Earth (Dungan and Rhodes, 1978; Sobolev and Shimizu, 1993; Sobolev, 1996; Eiler et al., 1998; Saal et al., 1998; Schiano et al., 1998; Shimizu, 1998; Sisson and Bronto, 1998; Sours-Page et al., 1999). The major element compositions of olivine-hosted melt inclusions are especially susceptible to post-entrapment modification, limiting our

* Corresponding author.

0009-2541/02/$ - see front matter © 2002 Published by Elsevier Science B.V.
PII: S0009-2541(01)00370-9

ability to accurately determine their initial compositions (Watson, 1976; Sobolev and Danyushevsky, 1994; Sobolev, 1996; Sobolev and Chaussidon, 1996; Danyushevsky et al., 2000; Gaetani and Watson, 2000). Although the effects of crystallization can be reasonably well accounted for through olivine-addition calculations, the combined effects of Fe–Mg exchange and diffusive re-equilibration with the host crystal have the potential to obscure the amount of post-entrapment crystallization that has actually occurred. Therefore, the extent to which the major element variability observed in olivine-hosted melt inclusions is truly representative of polybaric, near-fractional partial melting of mantle peridotite, rather than post-entrapment processes, is an important, unresolved issue (Nielsen et al., 1998).

Numerical simulations constrained by experimental data on olivine/melt equilibrium and the interdiffusion of Fe and Mg in magnesian olivine can be used to assess the capacity of post-entrapment processes to alter the major element compositions of olivine-hosted melt inclusions. Gaetani and Watson (2000) developed a finite-difference code to model the post-entrapment evolution of olivine-hosted melt inclusions, and used it to show that diffusive re-equilibration has the potential to significantly and irreversibly change the major element composition of an included melt. Here, we present a detailed description of the model, and use it to determine the extent to which near-fractional peridotite partial melts that become included in olivine within the melting regime are modified during transport to the surface.

2. Methods

2.1. Olivine/melt equilibrium

The model system consists of a spherical melt inclusion centered in a spherical olivine grain. The outer surface of the crystal is in contact with an external melt whose composition need not be the same as that of the included melt. Expressions describing the equilibrium distribution of FeO and of MgO between olivine and silicate melt are used to define the equilibrium conditions at both the inclusion/host interface and the outer surface of the olivine grain. These expressions were formulated starting from the equivalence of chemical potentials in coexisting phases. If the heat capacities (C_p) and the

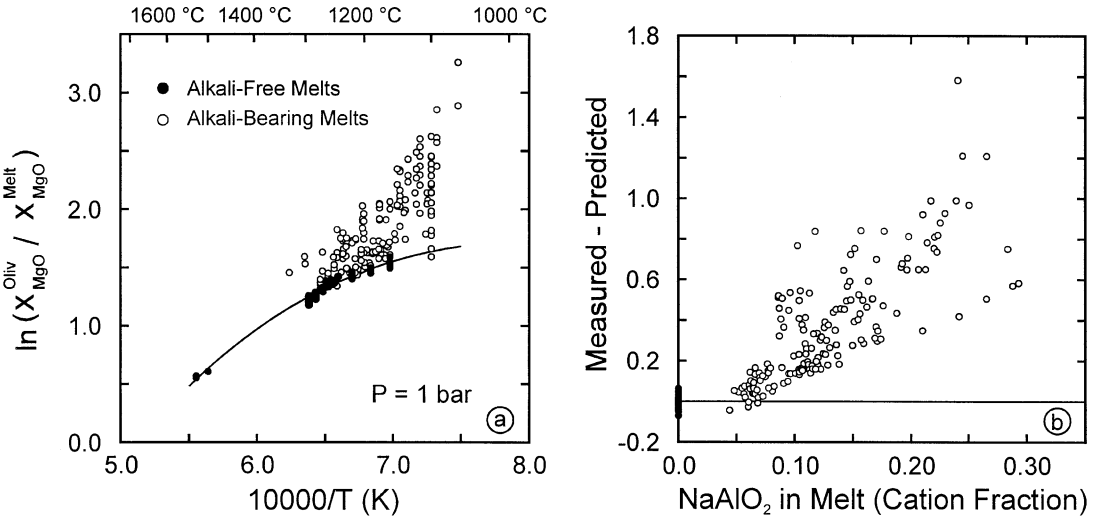

Fig. 1. (a) Plot illustrating the relationship between inverse temperature and the molar partitioning of MgO between olivine and both alkali-free (filled symbols) and alkali-bearing (open symbols) silicate melts at a pressure of 1 bar. Curve is a fit of data from alkali-free systems to Eq. (1). (b) Plot of $NaAlO_2$ component in the silicate melt (cation fraction) versus residuals from alkali-free temperature dependence at 1 bar illustrating the strong dependence of olivine/melt equilibrium on the alkali content of the liquid. Symbols are the same as in (a).

activity coefficient for component i in the olivine ($\gamma_i^{\text{Olivine}}$) are approximated as constants, and the effects of temperature (T) and pressure (P) on partial molar volume are assumed to be negligible, the natural logarithm of the ratio of the mole fraction of component i in olivine (X_i^{Olivine}) relative to that in the melt (X_i^{Melt}) can be expressed as:

$$\ln\frac{X_i^{\text{Olivine}}}{X_i^{\text{Melt}}} = C_0 + \frac{C_1}{T} + C_2\ln T + C_3\frac{(P-1)}{T} + \ln\gamma_i^{\text{Melt}} \quad (1)$$

where C_i are constants. The temperature terms in Eq. (1) can be used to describe the partitioning of MgO between olivine and alkali-free silicate melt at a pressure of 1 bar (Fig. 1a), but modeling natural basaltic systems requires an expression for non-ideality in the melt (Fig. 1b). Therefore, activity coefficients were formulated for FeO and for MgO by approximating the melt as a symmetric regular solution (Hildebrand and Scott, 1964):

$$RT\ln\gamma_{(\text{MgO,FeO})}^{\text{Melt}} = \sum_{i=1}^{n} W_{i(\text{MgO,FeO})}X_i - \frac{1}{2}\sum_{i-1}^{n}\sum_{j=1}^{n} W_{ij}X_iX_j \quad (2)$$

where W_{ij} are regression parameters describing the energy associated with interactions between liquid components.

Eqs. (1) and (2) were combined and calibrated using experimental data from the literature to provide a quantitative description of olivine/melt equilibrium. A total of 329 olivine–liquid pairs with analytical totals between 98.5 and 101.5 and olivine cation sums between 2.985 and 3.015 were recalculated into the components of Bottinga and Weill (1972) on a single-cation basis. The data set comprises experiments conducted on both analog and natural compositions, spanning temperatures of 1064 to 1950 °C and pressures of 1 bar to 70 kbar. On the basis of trial regression results, components that play similar melt-structural roles were grouped in order to simplify the activity coefficient expressions (Hirschmann et al., 1998). Figs. 2 and 3 demonstrate the precision with which the expressions recover the data in the calibration. The predictive capabilities of the expressions were tested against 35 experimentally produced basaltic melts saturated with olivine at 1 bar and 1100 to 1230 °C by Gaetani and Watson (2000).

The liquidus temperature of an olivine-saturated melt is estimated at any pressure by assuming that the coexisting olivine consists entirely of a forsterite–fayalite solid solution. The melt composition is recalculated, as described in Appendix A, and Eq. (1) is solved for X_i^{Oliv} as a function of temperature. The constraint provided by olivine stoichiometry is satisfied when $X_{\text{FeO}}^{\text{Oliv}}$ and $X_{\text{MgO}}^{\text{Oliv}}$ sum to 2/3, and this is taken as the liquidus temperature. This calculation can be efficiently carried out by minimizing the function:

$$f(T) = \left(2/3 - \left(X_{\text{FeO}}^{\text{Oliv}} + X_{\text{MgO}}^{\text{Oliv}}\right)\right)^2 \quad (3)$$

using a one-dimensional search algorithm, such as a golden section search (Press et al., 1989). A fractional liquid line of descent is calculated incrementally by removing a small amount of the equilibrium olivine (0.0005%), recalculating the fractionated liquid composition, and determining the new liquidus temperature. A bulk-equilibrium liquid line of descent is calculated by satisfying both the olivine stoichiometry constraint, using Eq. (1), and mass balance among the initial liquid (bulk composition), the fractionated liquid, and the equilibrium olivine at any given pressure and temperature. A polybaric liquid line of descent is calculated by formulating an expression describing pressure as a function of temperature ($P(T)$), and substituting it into Eq. (1). A comprehensive discussion of this approach to calculating mineral/melt equilibria and of its applications is found in Langmuir and Hanson (1981).

In the melt inclusion simulations carried out for this study, it is assumed that the external melt is saturated only with olivine. The addition of plagioclase and/or clinopyroxene to the crystallizing assemblage would complicate the calculations, but will not change any of the major conclusions significantly. It is also assumed that the external melt follows a bulk-equilibrium liquid line of descent. Although minor compositional gradients typically develop in the host olivine over the course of the simulations, indicating a departure from bulk equilibrium, the relationship between olivine composition and temperature during fractional crystallization is nearly indistinguishable

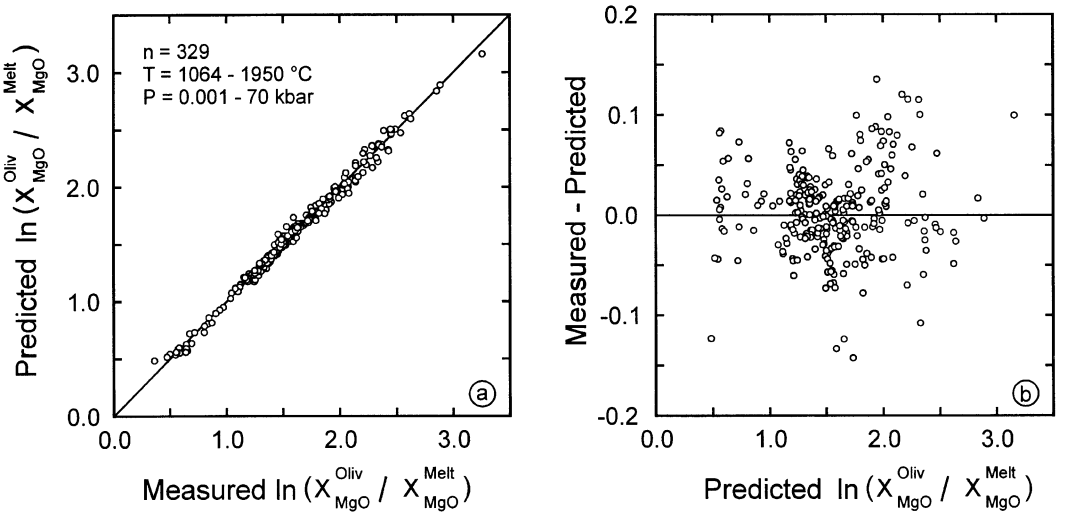

Fig. 2. Plot of measured versus predicted olivine/melt partition coefficients for MgO (molar) demonstrating the ability of the model described in the text to recover the calibration data. (b) Plot of predicted olivine/melt partition coefficients for MgO (molar) versus residuals for the calibration data shown in (a).

from the bulk-equilibrium case (Fig. 4). The composition of the outer boundary of the host olivine responds to changes in the fractionating external melt, but mass was not added because the amount of growth experienced by an individual crystal during cooling of a magma is probably small due to continuous nucleation of olivine (Marsh, 1988). In any case, the spherical geometry of the host crystal means that the increase in radius for a given amount of crystal growth will be small.

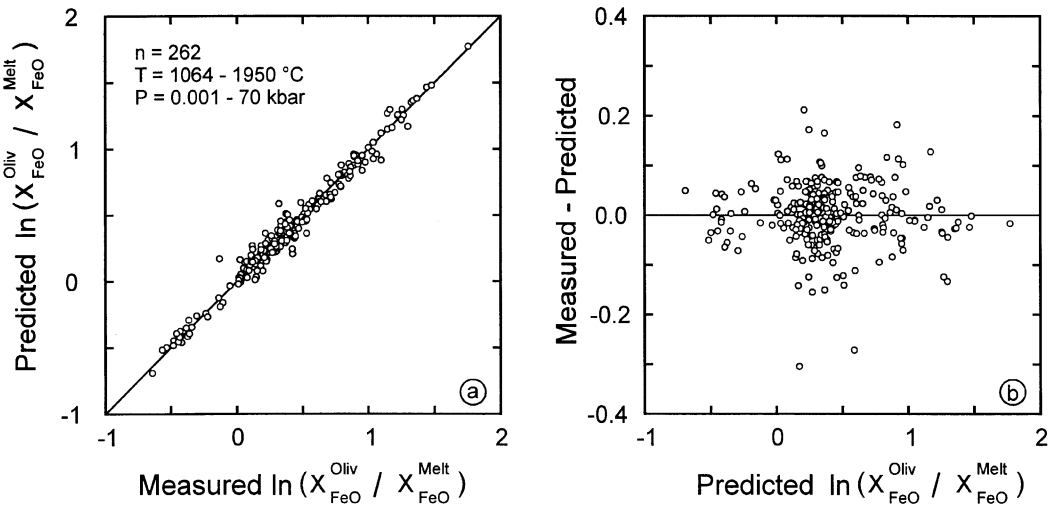

Fig. 3. Plot of measured versus predicted olivine/melt partition coefficients for FeO (molar) demonstrating the ability of the model described in the text to recover the calibration data. (b) Plot of predicted olivine/melt partition coefficients for FeO (molar) versus residuals for the calibration data shown in (a).

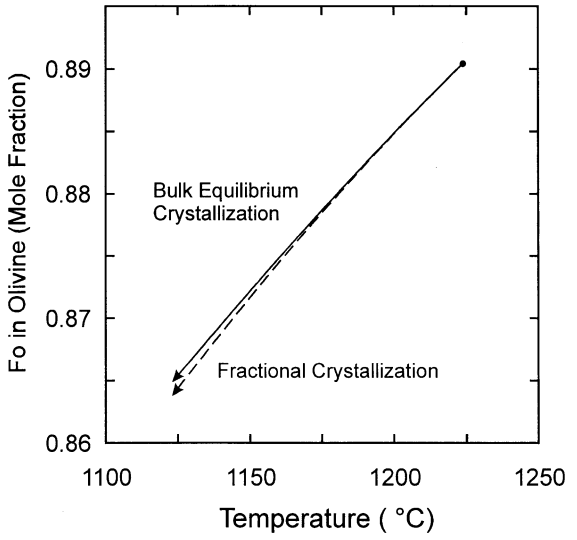

Fig. 4. Plot of temperature versus mole fraction of forsterite in olivine comparing the variation in olivine composition during bulk equilibrium (solid curve) and fractional (dashed curve) crystallization.

2.2. Interdiffusion of Fe and Mg in olivine and inclusion/host exchange

When the $P-T$ conditions of an olivine-hosted melt inclusion deviate from the conditions of entrapment, precipitation (or dissolution) of olivine is expected, and the new equilibrium olivine composition will differ from that of the original host according to the Fe and Mg partitioning equations discussed above and in Appendix A. Cooling of the system, for example, would result in a layer of new, more Fe-rich olivine at the inclusion/host interface. In the absence of diffusion in the olivine, this new layer would be chemically zoned in such a way as to reflect the extent of cooling, and its outer margin would mark the original inclusion/host interface. Clearly, the occurrence of Fe–Mg interdiffusion in the olivine could complicate this picture significantly, perhaps obscuring any record of the original inclusion/host interface and potentially allowing extensive, continuous exchange of Fe and Mg between the inclusion and its host. Unfortunately, even very simple diffusion calculations using existing experimental constraints on Fe–Mg interdiffusion rates can be used to show that the complex picture is more realistic: diffusion in olivine is simply too rapid to avoid extensive homogenization of the host olivine and significant inclusion/host exchange.

In the hope of understanding the exchange process in detail — and perhaps recovering some of the lost information — we developed a simple but versatile numerical approach to modeling diffusion in olivines containing basaltic inclusions. The approach incorporates standard iterative schemes described in numerous textbooks on numerical modeling; the details of these will be omitted so more attention can be given to particular pitfalls and aspects of our approach that are relatively unique.

As noted in the previous section, our model system is spherical melt inclusion centered within a spherical olivine crystal (Fig. 5). The volume occupied by olivine (in which Mg–Fe interdiffusion is modeled in detail) thus consists of a thick shell or mantle bounded at the inner surface by the melt inclusion

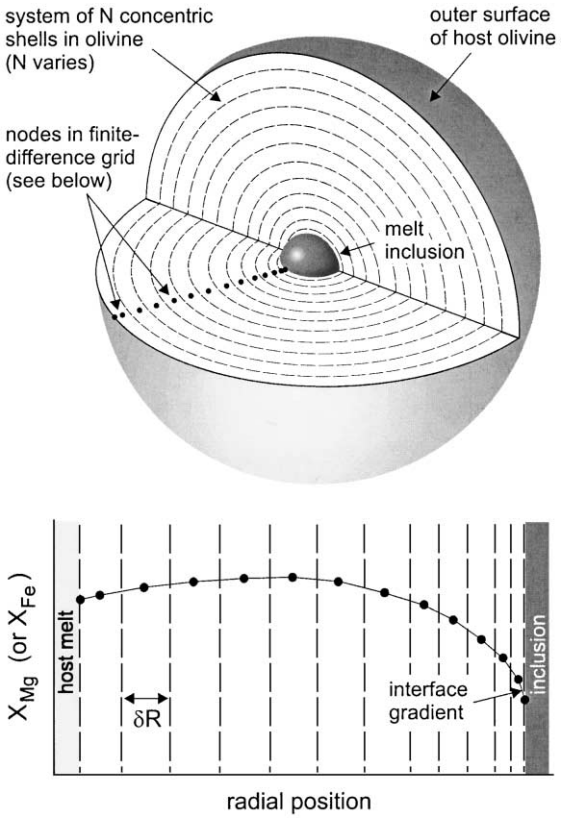

Fig. 5. Schematic illustration of the model system used for the numerical simulations. See text for discussion.

and on the outside by the host melt. The compositions of both the inner and outer boundaries change as the system evolves along a prescribed cooling or decompression path, in accordance with the Fe and Mg partitioning formulations discussed above and presented in Appendix A. The position of the inner (inclusion/host) boundary migrates in the spherical reference frame as olivine precipitates from the melt inclusion by uniform "plating" on the wall. The position of the outer boundary (olivine surface) is, for reasons noted previously, considered to be fixed.

The non-steady state equation describing diffusion within the spherical olivine is:

$$\frac{\partial X_i^{\text{Olivine}}}{\partial t} = D_{\text{Fe-Mg}}\left(\frac{\partial^2 X_i^{\text{Olivine}}}{\partial R^2} + \frac{2}{R}\frac{\partial X_i^{\text{Olivine}}}{\partial R}\right) \quad (4)$$

where X_i^{Olivine} is the mole fraction of Fe or Mg in the olivine, $D_{\text{Fe-Mg}}$ is the diffusivity governing Fe–Mg exchange, R is the radial distance from the center of the spherical system (i.e., the center of the melt inclusion) and t is time (see, e.g., Crank, 1975). The diffusive exchange process dictated by olivine stoichiometry necessitates that:

$$\left.\frac{\partial X_{\text{Fe}}^{\text{Olivine}}}{\partial t}\right|_{R=R_i} = -\left.\frac{\partial X_{\text{Mg}}^{\text{Olivine}}}{\partial t}\right|_{R=R_i} \quad (5)$$

where R_i represents a coordinate of interest within the olivine. Because our simulations incorporate changes in temperature over time, and because $D_{\text{Fe-Mg}}$ is temperature-dependent, $D_{\text{Fe-Mg}}=f(t)$ and must be continuously recalculated to accurately model the process of interest. We expressed the temperature dependence of Fe–Mg interdiffusion by the Arrhenius relation:

$$D_{\text{Fe-Mg}} = 8.0\times10^{-7}\exp(-29708/T)\ \text{m}^2\text{s}^{-1} \quad (6)$$

determined experimentally by Jurewicz and Watson (1988) for diffusion parallel to the c crystallographic axis of $\sim$Fo$_{90}$ olivine at an oxygen fugacity (f_{O_2}) along the fayalite–magnetic–quartz (FMQ) buffer (see Fig. 6). This diffusion law was adopted in preference to others (e.g., Buening and Buseck, 1973; Misener, 1974; Chakraborty, 1997) because the conditions of the Jurewicz–Watson experiments

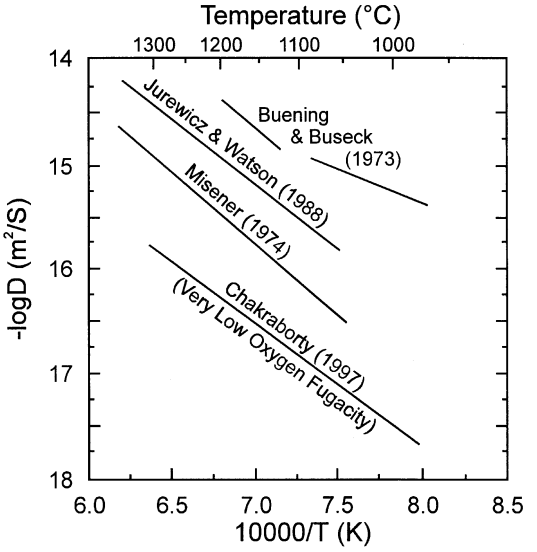

Fig. 6. Arrhenius plot comparing Fe–Mg interdiffusion coefficients for magnesian olivine as determined in four different experimental studies.

most closely resemble those pertaining to our models — in terms, that is, of olivine composition, P–T conditions and olivine–basalt exchange occurring during the interdiffusion process. It is important to note, also, that despite large *apparent* differences in reported $D_{\text{Fe-Mg}}$ values, the agreement among most experimental studies is actually quite good if the diffusivities are normalized to a comparable olivine composition and f_{O_2}. Chakraborty's (1997) Arrhenius relation gives diffusivities almost 2 orders of magnitude lower than those of Misener (1974) and Jurewicz and Watson (1988), but his study was done at an f_{O_2} of 10^{-12} bars, which is considerably more reducing than the conditions under which most basalts are thought to evolve (Christie et al., 1986). As Chakraborty (1997) noted, his data can be brought into virtual coincidence with those of Misener (1974) by taking into account the strong f_{O_2} dependence of $D_{\text{Fe-Mg}}$. Eq. (6) gives $D_{\text{Fe-Mg}}$ values roughly a factor of 3 higher than those of Misener (1974). As discussed by Gaetani and Watson (2000), such a difference is relatively unimportant to the broad conclusions that can be drawn from modeling of melt inclusion behavior, inasmuch as a factor of 3 change in D leads to a factor of only $\sqrt{3}$ difference in the characteristic diffusive transport distance. Viewed another way, the differences in

D_{Fe-Mg} between Jurewicz–Watson and Misener would lead to ~ 50 °C difference in 'Dodson' closure temperature (Dodson, 1973) of the Fe–Mg exchange process (reflecting, in part, the good agreement in activation energy for Fe–Mg interdiffusion among the different experimental studies). Various diffusion laws for Fe–Mg exchange in magnesian olivine are summarized in Fig. 6. Ultimately, our choice of the Jurewicz–Watson relation (Eq. (6)) was substantiated by our success in reproducing in a numerical simulation the measured diffusion field surrounding an olivine-hosted melt inclusion that we reheated in the laboratory (see Gaetani and Watson, 2000).

Olivine shows some anisotropy with respect to diffusion of Fe, Mg and other cations (Buening and Buseck, 1973; Misener, 1974; Jurewicz and Watson, 1988), with diffusion along the *c*-axis fastest in most cases (by a factor of ~ 5 relative to the slowest diffusion direction). Because of the much greater complexity and small gain of modeling diffusion in a triaxial ellipsoid, we have ignored olivine's diffusive anisotropy in our modeling, as implied in our use of Eq. (4) and a spherical model system.

We employ an 'explicit' finite-difference method in all simulations. In this method, a single unknown composition at a specific coordinate is expressed directly in terms of spatially adjacent known values at each time step. This is in contrast with the 'implicit' method, in which compositions at several contiguous points are computed together in a given time step by solution of a set of simultaneous equations. The implicit method has the advantage that it is inherently stable (it cannot develop compositional oscillations with rapidly expanding errors) and allows the use of larger time steps, leading to greater computational efficiency. Computational speed was not a significant issue in our simulations, and we found it easier to cope with the changing boundary conditions and migration of the inner (inclusion/host) boundary using the explicit method. For general discussions of numerical approaches in diffusion, see Crank (1975), or any text on numerical solution of differential equations (e.g., Sewell, 1988).

We use a straightforward approach to setting up a 'grid' for numerical computation, the density of which is scaled to the requirements of the specific simulation. For modeling inclusion/host interaction during cooling at "subsurface" conditions (say, < 1 °C/year; as opposed to much faster "eruptive" cooling rates or laboratory re-heating), the olivine volume is divided into 12 concentric volume elements (shells) of thickness scaled to the overall thickness of the olivine mantle (see Fig. 5). The radial thickness δR of each shell is also scaled to its proximity to the melt inclusion, those closest to the inclusion being 1/4 the thickness of the outermost shells. This strategy affords better coverage of Mg–Fe concentration profiles near the melt inclusion where the steepest gradients are expected due to olivine precipitation and concurrent Fe–Mg exchange with the melt inclusion. The "slow-cooling" numerical grid thus consists of 14 node points, including those within each of the 12 volume elements plus the inner and outer boundaries of the olivine mantle. The radial node location within each shell is considered to be where half the mass of the shell lies "inside" (i.e., at smaller R) and half "outside" the node point (if R is very large relative to the shell thickness δR, this "mass-centered" position approaches the point half-way between the inner and outer bounding surfaces of the shell, i.e., at $\delta R/2$ within the shell).

In order to establish that 14 nodes are sufficient to accurately represent the processes of interest, we ran numerous comparisons against more densely gridded olivines, one of which is illustrated in Fig. 7. The simulations represented in the figure involve "subsurface" cooling of a 1-mm-diameter olivine containing a melt inclusion initially 100 μm in diameter. The simulations are initiated at 1224 °C where the inclusion is in equilibrium with olivine of composition $Fo_{89.1}$, and cooling is allowed to proceed for 100 years at 1 °C/year with a time step of 0.0001 years. The solid crosses in Fig. 7 show the final composition gradient in a 14-node olivine. For comparison, the open circles show the results of a similar simulation run with a 50-node olivine cooled in slightly shorter time steps of 0.00005 years. The final olivine composition profiles of the two simulations are virtually indistinguishable, the concentrations at any given radial position being the same to at least the fifth decimal place in $X_{MgO}^{Olivine}$. Even more significant in the context of our specific objectives is that the final melt inclusion compositions are identical for all intents and purposes (see inset table on Fig. 7).

For simulations involving rapid geologic cooling (e.g., 50 °C/h) or laboratory re-heating, we "re-grid"

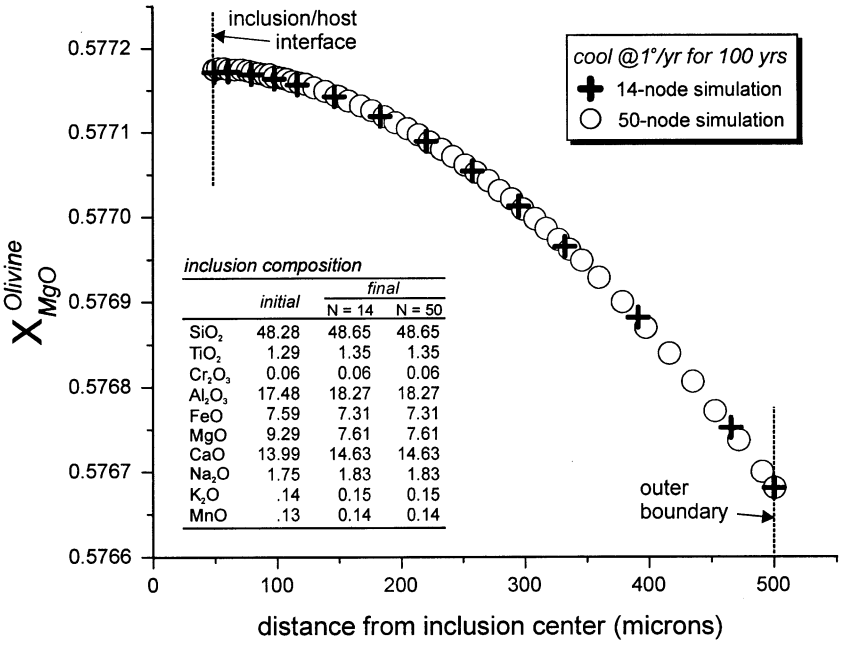

Fig. 7. Comparison of duplicate numerical simulations run with different numbers of nodes in the finite-difference array (14 versus 50). The results are virtually indistinguishable in terms of both the final composition profile in the olivine (crosses versus circle) and the final composition of the melt inclusion (inset table). See text for further discussion.

the olivine volume near the melt inclusion to a higher density in order to capture the details of the steep concentration gradients produced by rapid temperature changes. This re-gridding is also advantageous for accurate estimation of the fluxes of Fe and Mg at the inclusion/host interface (see below).

The main inputs for a simulation are the initial composition and size of the melt inclusion to be modeled, the size of the host olivine, and the desired cooling path, expressed as a constant rate of cooling. The initial (uniform) composition of the olivine is computed by assuming equilibrium with the melt inclusion and applying the Mg and Fe partitioning equations presented in Appendix A (along with the additional stoichiometric constraints that the Mg and Fe single-cation mole fractions must sum to 2/3 in olivine). A simulation is initiated with a short time step along the desired cooling path, with ΔT (K) generally falling in the range 10^{-6} to 10^{-4}. This small ΔT forces crystallization of new olivine on the melt inclusion wall. The composition of the newly precipitated olivine is given by our Fe–Mg partitioning equations, and its mass is estimated (initially) from a crystallization rate, $\mathrm{d}F/\mathrm{d}T$, derived from published phase equilibrium studies (F is the fraction of melt remaining). To maintain numerical stability, the olivine precipitated during a single time step is not treated as an infinitesimally thin layer of new olivine on the melt inclusion wall; rather, the appropriate number of moles of olivine components are incorporated into the innermost volume element of the host olivine, which grows inward accordingly (we also recalculate the density of the innermost volume element, though the time-integrated change is exceedingly small). The melt inclusion is simultaneously debited the components converted into olivine. Because the composition of the innermost shell of the olivine changes due to precipitation, a composition gradient develops in the olivine and Fe–Mg interdiffusion ensues.

Subsequent t–T steps are analogous to the first: decrease $T \rightarrow$ crystallize olivine $\rightarrow$ adjust inclusion composition $\rightarrow$ interdiffuse Fe and Mg in the olivine. The only added complexity as time increases is that the gradient in olivine composition near the inclusion wall causes a *diffusive* exchange between the olivine and the

inclusion that accompanies the transfer of olivine components via crystallization. Diffusion and crystallization must exactly balance one another so as to maintain Fe–Mg partitioning equilibrium at the inclusion/olivine interface. The crystallization rate, dF/dT, is an unknown function of time and temperature whose value depends on the momentary rate of diffusive exchange. We address this complication by dynamically adjusting dF/dT with each time step to achieve a match between the observed Fe–Mg exchange coefficient ($K_D^{Fe-Mg} = X_{FeO}^{Oliv} X_{MgO}^{Melt} / X_{MgO}^{Oliv} X_{Feo}^{Melt}$) at the inclusion/host interface and the value expected from the equilibrium partitioning equations. In effect, we "steer" the crystallization of olivine to maintain partitioning equilibrium in the presence of diffusive exchange. This steering is accomplished by comparing the expected and observed K_D^{Fe-Mg} values at each time step and nudging the crystallization rate one way or the other (in proportion to the magnitude of the deviation) to bring the values into coincidence. The expected and observed exchange partition coefficients are monitored continuously during a simulation, and the values periodically saved to a file for later inspection.

Although the outer boundary of the olivine (in contact with the host melt) is held fixed in space as the system cools, diffusive Fe–Mg exchange at this boundary is incorporated into the simulations, as required for the melt inclusion to communicate with the external melt.

The coupling of crystallization and diffusion processes in our simulations makes it difficult to predict a priori the criteria for numerical stability. Our approach is to attempt progressively longer time steps until instability becomes obvious in the continuous graphical display; we then decrease the time step by a factor of 10. We also take several precautions to insure accuracy, one of which is to model diffusion of Fe and Mg independently — rather than just assume that Eq. (5) holds — and then check the olivine stoichiometry at every node point after the simulation is complete. Our simulations maintain olivine stoichiometry, with independent Fe and Mg diffusion, to the sixth or seventh decimal place in the value of Fe + Mg at every node point. As an additional check for accuracy, we incorporate into each simulation a "before and after" inventory of all components. In general, the oxides initially present in the melt inclusion are accounted for to within 0.02%; the total moles of FeO and MgO in the system (including those exchanged with the host melt) are recoverable to within $\sim 0.1\%$ for simulations involving "subsurface" cooling rates, and to within $\sim 1\%$ for simulations of rapid heating or cooling in which the gradients are much steeper. A significant source of error is thought to be in the (spherical) numerical integration of the diffusion profiles in the olivines.

The finite-difference method is accurate to essentially any degree desired in modeling processes involving only diffusion. The accuracy depends upon the size of the time steps and distance elements, and hence on some ratio involving the capability of the computer and the patience of the modeler. Overall accuracy is more problematic when — as in these melt inclusion models — interface fluxes determine the course and outcome of the process of interest. Consider, for example, the fact that the instantaneous fluxes of Fe and Mg at the olivine interface determine the rate of change of the melt inclusion composition at any time in during a simulation. In the case of Mg, for example,

$$\frac{dX_{Mg}^{Melt}}{dt} = -D_{Fe-Mg} \left.\frac{\partial X_{Mg}^{Olivine}}{\partial R}\right|_{R=R_{incl}} \cdot \frac{3}{R_{incl}} \qquad (7)$$

where R_{incl} is the radius of the melt inclusion at time t. When the derivative $\partial X/\partial R$ taken at the interface ("interface gradient" in Fig. 5) is approximated in finite-difference form, its value depends to some extent on the value δR. Accordingly, the surface flux $[= -D(\partial X/\partial R)]$ and the rate of change of X_{Mg} in the melt inclusion will also depend upon the choice of δR. When integrated over the course of an entire simulation, this effect can be significant to the outcome. A reasonable precaution against serious error is to run simulations using progressively smaller δR until there is no perceptible change in the time-integrated effect (see preceding discussion of grid density and Fig. 7).

In all our simulations, we assume diffusion in the melt to be infinitely fast in comparison to the processes of interest in this study. In other words, the inclusions are considered to be homogeneous at all times. This assumption is rigorously testable through cooling simulations incorporating appropriate diffusivities for Fe and Mg in the melt. It can be shown that

a melt inclusion of 50-μm radius cooling at 100 °C/h (1250 to 1150 °C) and in continuous surface equilibrium with olivine develops a center-to-margin concentration difference of only 0.4% relative, which is not detectable by electron microprobe (even for very fast cooling–e.g. at 1000 °C/h—the difference is only 4% relative). For "geologic" cooling rates, melt inclusions are well mixed by diffusion.

3. The transition from closed to open system behavior in olivine-hosted melt inclusions

The variables that control the extent of diffusive re-equilibration experienced by a melt inclusion are those that define the characteristic lengthscale and timescale for diffusive transport: cooling rate, inclusion radius, olivine radius, and, for a xenocryst, residence time (Qin et al., 1992; Danyushevsky et al., 2000; Gaetani and Watson, 2000). To illustrate the transition from closed system to open system behavior as a function of cooling rate, a series of simulations was carried out in which a 200-μm-diameter melt inclusion centered within a 1-mm-diameter olivine was cooled from 1224 to 1174 °C over timescales ranging from 30 min to 57 years. The compositional gradients produced in the host olivine as a result of these cooling histories are shown in Fig. 8.

Prior to cooling, the inclusion is in equilibrium with both the host olivine, whose composition is represented by a horizontal line, and the external melt. If the cooling rate is on the order of ~100 °C/h, as might be expected during cooling of a lava flow, the temperature decrease drives crystallization of new olivine that is increasingly Fe-rich by a process that approaches fractional crystallization. The short timescale over which cooling takes place does not allow for significant diffusive transport within the olivine, so that steep compositional gradients develop adjacent to both the inclusion and the surface of the olivine grain. The value of inclusion analyses as indicators of trapped melt composition is not totally compromised in this case, because olivine-addition calculations can be used to correct the inclusion composition for the

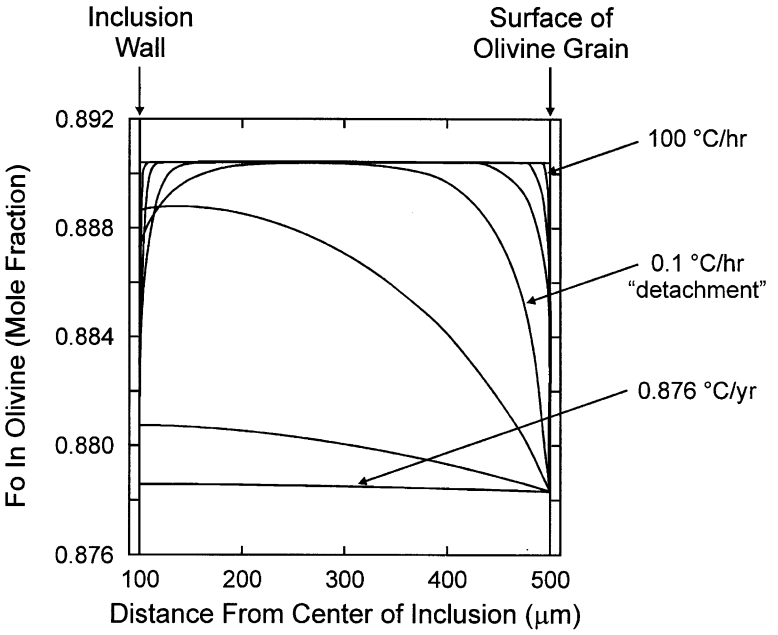

Fig. 8. Plot of distance from the center of an olivine-hosted melt inclusion versus forsterite content of the host olivine showing results from simulations in which a 200-μm diameter melt inclusion hosted in a 1-mm-diameter olivine was cooled from 1224 to 1174 °C at cooling rates of 100, 10, 1, and 0.1 °C/h, and 87.6, 8.76, and 0.876 °C/year. The inclusion composition used for the simulations is from column 2 of Table 1 in Gaetani and Watson (2000).

effects of crystallization. Compositional gradients corresponding to rapid cooling are typical of the olivine surrounding melt inclusions recovered from sub-aerial lava flows (e.g., Anderson, 1974; Gaetani and Watson, 2000).

Analytic solutions to the heat conduction equation indicate that cooling rates on the order of ~ 0.1 °C/h may be experienced by an olivine-hosted melt inclusion within a dike (Jaeger, 1968). At these cooling rates, diffusive transport within the host olivine becomes significant enough that broad compositional gradients develop. For the parameters used in our simulations, the diffusion profile adjacent to an inclusion that has cooled at 0.1 °C/h for 500 h has intersected that adjacent to the surface of the olivine grain, signaling communication of the inclusion with the melt surrounding the host olivine (i.e., open system behavior). This critical stage was termed "detachment" by Watson and Cherniak (1997), in reference to the point at which the radial diffusion profile separates from the initial (uniform) profile along its entire length. Once the inclusion has begun to behave as an open system, the composition of the host olivine at the time of entrapment cannot be determined from a microprobe analysis of the present crystal at any location within its volume. Therefore, olivine-addition calculations can no longer be used to obtain a reliable estimate of the initial major element composition of the inclusion. Cooling rates on the order of ~ 0.1 °C/year or less are estimated for crustal magma chamber (e.g., Cooper et al., 2001), indicating that olivine-hosted melt inclusions are able to maintain a close approach to Fe–Mg exchange equilibrium with the external melt as the system cools. The extent to which the initial composition of a given melt inclusion has been modified by crystallization and diffusive re-equilibration depends upon the extent to which the system has cooled between the time of entrapment and eruption of the olivine phenocryst containing the inclusion. Any compositional gradients that may develop in the host olivine during cooling at these conditions will be negligible, so that no record of this process will be preserved.

The specific cooling rate at which an inclusion becomes an open system (i.e., at which detachment occurs) depends upon, among other things, the thickness of the olivine surrounding the inclusion and the duration of the cooling event, as illustrated in Fig. 9. Filled circles represent combinations of olivine thickness and cooling rate for which simulation results indicate that a 200-μm-diameter melt inclusion, cooled by 100 °C, has just become open to communication with the external melt. The shaded region represents conditions at which the major element composition of the inclusion has been compromised. Also shown are curves calculated for temperature drops of 100 °C (solid), 50 °C (dashed), and 25 °C (dotted) using the approximation:

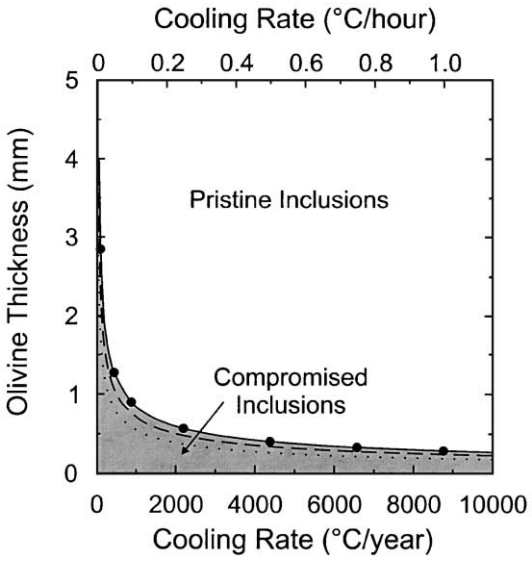

Fig. 9. Plot of olivine thickness (olivine radius minus melt inclusion radius) versus cooling rate showing the transition from closed to open system behavior on the basis of simulation results (filled circles) or calculated from Eq. (8) (curves) for cooling intervals of 100 °C (filled circles; solid curve), 50 °C (dashed curve), and 25 °C (dotted curve). Shaded region represents conditions at which an inclusion behaves as an open system for a temperature drop of 100 °C.

$$\frac{Dt}{x^2} \approx 0.00429 \tag{8}$$

where D is diffusivity, calculated from Eq. (6) using the mean temperature for the cooling interval of interest, t is time, and x is the thickness of olivine surrounding the inclusion. This approximation is similar to that used by Watson and Cherniak (1997) to calculate the maximum time for preservation of the original $^{18}O/^{16}O$ at the center of an overgrowth zircon rim, and can be used to estimate the conditions

required for a particular inclusion to preserve an accurate record of its initial composition. The most important aspects of the results presented in Fig. 9 are that (1) if a melt inclusion is within ~ 500 μm of the surface of an olivine grain, it is unlikely to behave as a closed system; (2) inclusions hosted in olivine grains that are several mm in diameter will behave as open systems at cooling rates thought to be characteristic of magma chambers; (3) these conclusions are only weakly dependent upon the size of the temperature drop because the transport distance scales as the square root of time and diffusivity.

4. Post-entrapment evolution of near-fractional partial melts

Partial melts are efficiently extracted from residual peridotite beneath spreading ridges in the oceanic mantle (Klein and Langmuir, 1987; Johnson et al., 1990; Sobolev and Shimizu, 1993). Once near-fractional melts have segregated from the residual solid, their major element compositions are susceptible to modification by a number of different processes, including magma mixing, crystal fractionation, and magma–wall rock interaction (e.g., Walker et al., 1979; Grove et al., 1992; Kelemen et al., 1997). Olivine-hosted melt inclusions are physically isolated from these processes, preserving at least some of the compositional diversity produced by the melting process. Although most sampled melt inclusions are likely to have formed at crustal levels, there is evidence for the existence of inclusions that formed at upper mantle pressure and temperature conditions (Sobolev, 1996; Shimizu, 1998). Inclusions formed within the melting regime are likely to be the most representative of near-fractional melts because the time between melt generation and inclusion formation is minimized. Here, we use the model for olivine-hosted melt inclusions described in previous sections to estimate the extent to which an inclusion formed within the melting regime and transported to the surface along a mantle geotherm preserves its initial major element composition.

First, incremental batch melts of spinel lherzolite were calculated for ascent along an adiabat intersect-

Table 1
Compositions of silicate melts referred to in this study

Melt	P	F	SiO_2	TiO_2	Al_2O_3	Cr_2O_3	FeO	MnO	MgO	CaO	Na_2O	K_2O
PM	20	0.0100	47.65	1.59	16.92	0.09	9.48	–	10.95	8.70	4.03	0.60
PM	16	0.0199	48.64	1.52	16.64	0.09	8.91	–	10.34	9.20	4.57	0.09
PM	15	0.0297	48.83	1.41	16.75	0.09	8.17	–	10.78	9.86	4.10	0.01
PM	14	0.0394	49.10	1.30	17.01	0.09	7.39	–	11.04	10.44	3.62	0.00
PM	13	0.0490	49.32	1.20	17.23	0.09	6.84	–	11.21	10.98	3.12	0.00
PM	12	0.0585	49.52	1.11	17.40	0.09	6.45	–	11.30	11.49	2.64	0.00
PM	11	0.0679	49.72	1.02	17.53	0.09	6.19	–	11.32	11.96	2.16	0.00
PM	10	0.0773	49.96	0.94	17.65	0.09	6.01	–	11.26	12.38	1.72	0.00
PM	9	0.0865	50.25	0.86	17.77	0.09	5.86	–	11.10	12.75	1.32	0.00
PM	8	0.0956	50.63	0.79	17.90	0.10	5.71	–	10.84	13.07	0.96	0.00
PM	7	0.1047	51.15	0.73	18.08	0.10	5.50	–	10.46	13.32	0.67	0.00
PM	6	0.1136	51.82	0.67	18.31	0.10	5.19	–	9.97	13.51	0.43	0.00
PM	5	0.1225	52.68	0.61	18.59	0.10	4.79	–	9.32	13.64	0.26	0.00
PM	4	0.1313	53.76	0.56	18.94	0.10	4.28	–	8.52	13.70	0.14	0.00
PM	3	0.1399	55.12	0.51	19.35	0.10	3.66	–	7.50	13.68	0.07	0.00
Σ	–	0.1399	50.46	1.00	17.70	0.09	6.36	–	10.43	11.84	2.05	0.05
EM	5	0.0297	49.61	1.54	18.27	0.10	7.74	–	7.52	10.75	4.47	0.01
MI	5	0.0297	49.60	1.52	18.03	0.10	7.14	–	8.57	10.62	4.41	0.01

Compositions are reported in weight percent. Initial peridotite composition is H&Z dep 1 from Kinzler (1997). P = pressure in kilobars. F = cumulative melt fraction relative to initial peridotite mass. PM = near-fractional peridotite partial melt calculated using the method of Kinzler (1997). Σ = aggregation of near-fractional partial melts. EM = external melt composition from melt inclusion simulation. MI = melt inclusion composition from simulation.

ing the anhydrous peridotite solidus at 20 kbar. Beginning with a depleted oceanic upper mantle peridotite, the composition of a 1% batch melt was calculated at 20 kbar using the method of Kinzler (1997). The Fe/Mg ratio of the equilibrium olivine was assumed to be equivalent to that of the bulk peridotite, and the equilibrium K_D^{Fe-Mg} was defined by our model for olivine/melt equilibrium. All of the melt was extracted from the peridotite after 1% partial melting, then mass balance was used to calculate the composition of the residual solid. Pressure was decreased by 1 kbar, and a 1% batch melt was calculated for the new bulk composition at the new pressure. This process was repeated until the final 1% partial melt was generated at 3 kbar. Extraction of the first increment of melt, at 20 kbar, raised the solidus temperature of the residual peridotite above the mantle geotherm, so that additional melt was not produced until the pressure reached 16 kbar. The incremental melt compositions calculated for decompression from 20 to 3 kbar are reported in Table 1, along with the composition of a liquid formed by aggregating the incremental melts.

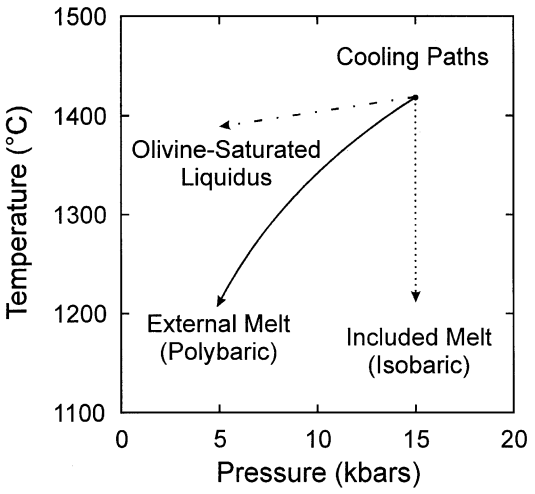

Fig. 10. Pressure versus temperature plot comparing the cooling paths followed by an olivine-hosted melt inclusion (dotted line) and the external melt (solid curve) during the simulation discussed in the text. Shown for comparison (dash-dot line) is the slope of the experimentally determined olivine-saturated liquidus for a mid-ocean ridge basalt (Bender et al., 1978).

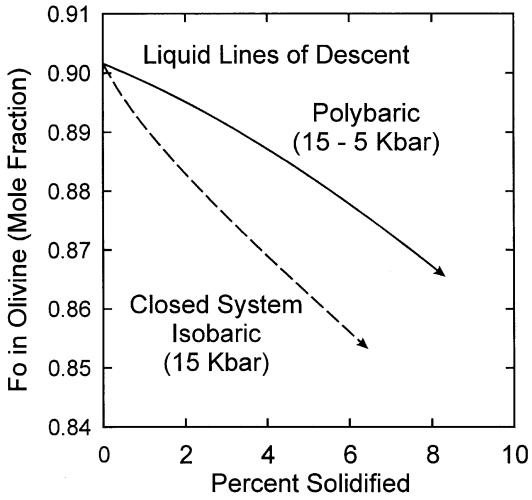

Fig. 11. Plot comparing the variation in olivine composition during crystallization of a basalt under isobaric (15 kbar) versus polybaric (15 to 5 kbar) conditions. Cooling paths are those shown in Fig. 10.

Once the peridotite melting calculations had been carried out, a melt inclusion simulation was run in which the increment of melt formed at 15 kbar was trapped as a 100-μm-diameter inclusion within a 2-mm-diameter olivine, then transported to 5 kbar along the melting regime geotherm shown by the solid curve in Fig. 10. Although the melt inclusion will undergo at least some percentage of the decompression experienced by the external surface of the host olivine (Zhang, 1998; Schiano and Bourdon, 1999), we chose to examine the endmember case in which the pressure of entrapment is preserved (dotted line in Fig. 10). This was done because complete decompression of the inclusion will cause it to follow the same liquid line of descent as the external melt, while incomplete decompression results in compositional to the inclusion that are intermediate to the endmember cases. Although the appropriate cooling rate is likely to be lower, 0.5 °C/year was chosen for the simulation because it produced complete equilibration of the host olivine.

Our calculations indicate that, even if diffusive transport through the host olivine is ignored, an inclusion trapped at upper mantle conditions must undergo significant modification in transit to the surface. The experimentally determined olivine-satu-

rated liquidus for basalt (dash-dot curve in Fig. 10) is shallower than the melting regime geotherm (solid curve in Fig. 10), so that olivine will crystallize from both the inclusion and the external melt during ascent. In the absence of diffusive exchange with the host olivine, the pressure difference between the inclusion and the external melt causes each to follow a slightly different liquid line of descent; olivine crystallizing from the external melt is more forsteritic (Fig. 11). Although olivine crystallization modifies the inclusion composition in the hypothetical closed-system case, these changes can be accounted for with reasonable accuracy through olivine-addition calculations.

The rapid interdiffusivity of Fe and Mg in the host olivine results in compositional changes to the included melt (dotted curve in Fig. 12) that differ significantly from the closed-system case just discussed. The mass of the external melt dominates the system, so that the composition of the host olivine will be controlled by the polybaric liquid of descent. The composition of the inclusion is forced to remain in equilibrium with the composition of host olivine at a pressure of 15 kbar through a combination of crystallization and diffusive exchange. The net result is that the inclusion follows a compositional path (dotted curve in Fig. 12) that is not consistent with either polybaric (solid curve in Fig. 12) or closed system isobaric (dashed curve in Fig. 12) crystallization of olivine.

In summary, our model predicts that the composition of an olivine-hosted melt inclusion will be modified substantially during transit through the melting regime. It is difficult to determine how effective olivine calculations are for recovering the initial composition of the inclusion until the physics of the problem are completely understood. The inclusion is likely to undergo some amount of decompression, and if the final pressure gradient within the host olivine is small, the compositional path followed by the inclusion can be approximated by a polybaric liquid of descent. If the host olivine is capable of preserving a substantial pressure gradient, the initial composition of the inclusion cannot be reliably recovered.

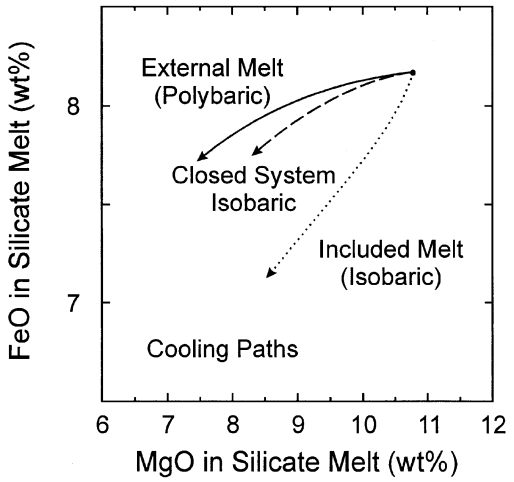

Fig. 12. Plot of MgO versus FeO (both in wt.%) comparing the different liquid compositional paths discussed in the text. Solid curve represents the polybaric liquid line of descent followed by the external melt during the melt inclusion simulation. Dotted curve represents the compositional path followed by the melt inclusion during the simulation. Dashed curve represents the path that the inclusion would have followed if it retained its entrapment pressure of 15 kbar, but there was no diffusive exchange with the host olivine.

Acknowledgements

The authors are grateful to an anonymous referee for thoughtful comments, and to E. Hauri for his editorial handling of the paper. We thank A.V. Sobolev for encouraging us to this special issue of Chemical Geology. S.R. Hart provided the original motivation for exploring the re-equilibration of melt inclusions during transport through the upper mantle (although he now believes we engaged in a little overkill). This work was supported by the National Science Foundation under Grants no. EAR-9804794 and EAR-0087525.

Appendix A: *Model for olivine/melt equilibrium*

The model for olivine/melt equilibrium discussed in the text requires that melt compositions be cast in the components of Bottinga and Weill (1972). The calculations are carried out on a single-cation, or gram-cation, basis to provide conservative units (Brady and Stout, 1980). After converting the melt composition

Table A1
Regression coefficients for olivine/melt partitioning expressions

C_0	C_1	C_2	C_3	C_4	C_5	C_6	C_7	C_8	C_9	C_{10}	C_{11}	C_{12}	C_{13}
MgO partitioning													
−22.1733	1379.3	2.8095	−8.09 × 10e−3	7377.7	3854.1	8546.9	11 470.1	−11 614.0	−14 006.4	−12 233.1	9927.2	−3087.1	−8048.5
FeO partitioning													
−0.12445	3826.4	−0.3372	15.46 × 10e−3	4682.9	−1330.6	2450.1	5933.8	−11 905.8	−14 006.4	−12 233.1	9046.2	−3150.4	−8048.5

Sources of data used in regression: Grove et al. (1982); Grove and Bryan (1983); Sack et al. (1987); Tormey et al. (1987); Libourel et al. (1989); Grove et al. (1990); Pan and Longhi (1990); Bartels et al. (1991); Shi and Libourel (1991); Kinzler and Grove (1992); Shi (1993); Kinzler (1997); Gaetani and Grove (1998); Milholland and Presnall (1998); Walter (1998); Libourel (1999); Gudfinnsson and Presnall (2000).

from weight units to cation units, it is recalculated into oxide and aluminate components as follows:

$$SiO_2 = SiO_2 + PO_{2.5};\ TiO_2 = TiO_2;\ CrO_{1.5} = CrO_{1.5}$$

$$FeO = FeO + FeO_{1.5};\ MnO = MnO;\ MgO = MgO$$

$$KAlO_2 = 2 \times KO_{0.5};\ AlO_{1.5} = AlO_{1.5} - KO_{0.5}$$

$$NaAlO_2 = 2 \times NaO_{0.5};\ AlO_{1.5} = AlO_{1.5} - NaO_{0.5}$$

$$CaAl_2O_4 = \frac{3}{2} \times AlO_{1.5},$$

$$CaO = CaO - \frac{1}{3} \times CaAl_2O_4$$

The melt composition is then normalized to 1. The model is not calibrated for melts that do not contain a CaO component.

Once the melt composition has been cast into Bottinga–Weill components, they are grouped as follows:

$$S = SiO_2;\ C = CaAl_2O_4;\ A = NaAlO_2 + KAlO_2$$

$$NM_{MgO} = TiO_2 + CrO_{1.5} + FeO + MnO + CaO$$

$$NM_{FeO} = TiO_2 + CrO_{1.5} + MgO + MnO + CaO$$

and substituted into expressions describing olivine/melt partitioning of the form:

$$\ln\frac{X_i^{Oliv}}{X_i^{Melt}} = C_0 + \frac{C_1}{T} + C_2\ln T + \frac{C_3(P-1)}{T} + \frac{1}{T}\left[C_4\left(S - SX_i^{Melt}\right) + C_5\left(NM_i - NM_iX_i^{Melt}\right) + C_6\left(C - CX_i^{Melt}\right) + C_7\left(A - AX_i^{Melt}\right) + C_8SNM_i + C_9SC + C_{10}SA + C_{11}NM_iC + C_{12}NM_iA + C_{13}AC\right] \quad (A1)$$

where T is temperature in Kelvin, P is pressure in bars, C_n are the regression coefficients given in Table A1, and i is either MgO or FeO.

References

Anderson Jr., A.T., 1974. Evidence for a picritic, volatile-rich magma beneath Mt. Shasta, California. J. Petrol. 15, 243–267.

Bartels, K.S., Kinzler, R.J., Grove, T.L., 1991. High pressure phase relations of primitive high-alumina basalts from Medicine Lake Volcano, Northern California. Contrib. Mineral. Petrol. 108, 253–270.

Bender, J.F., Hodges, F.N., Bence, A.E., 1978. Petrogenesis of basalts from the Project FAMOUS area: experimental study from 0 to 15 kbar. Earth Planet. Sci. Lett. 41, 277–302.

Bottinga, Y., Weill, D.F., 1972. The viscosity of magmatic silicate liquids: a model for calculation. Am. J. Sci. 272, 438–475.

Brady, J.B., Stout, J.H., 1980. Normalizations of thermodynamic properties and some implications for graphical and analytical problems in petrology. Am. J. Sci. 280, 173–189.

Buening, D.K., Buseck, P.R., 1973. Fe–Mg lattice diffusion in olivine. J. Geophys. Res. 78, 6852–6862.

Chakraborty, S., 1997. Rates and mechanisms of Fe–Mg interdiffusion in olivine at 980–1300 °C. J. Geophys. Res. 102, 12317–12331.

Christie, D.M., Carmichael, I.S.E., Langmuir, C.H., 1986. Oxidation state of mid-ocean ridge basalt glasses. Earth Planet. Sci. Lett. 79, 397–411.

Cooper, K.M., Reid, M.R., Murell, M.T., Clague, D.A., 2001. Crystal and magma residence at Kilauea Volcano, Hawaii: $^{230}Th-^{226}Ra$ dating of the 1955 east rift eruption. Earth Planet. Sci. Lett. 184, 703–718.

Crank, J., 1975. The Mathematics of Diffusion. Clarendon Press, Oxford, 414 pp.

Danyushevsky, L.V., Della-Pasqua, F.N., Sokolov, S., 2000. Re-equilibration of melt inclusions trapped by magnesian olivine phenocrysts from subduction-related magmas: petrological implications. Contrib. Mineral. Petrol. 138, 68–83.

Dodson, M., 1973. Closure temperature in cooling geochronological and petrological systems. Contrib. Mineral. Petrol. 40, 259–274.

Dungan, M.A., Rhodes, J.M., 1978. Residual glasses and melt inclusions in basalts from DSDP Legs 45 and 46: evidence for magma mixing. Contrib. Mineral. Petrol. 67, 417–431.

Eiler, J.M., McInnes, B., Valley, J.W., Graham, C.M., Stolper, E.M., 1998. Oxygen isotope evidence for slab-derived fluids in the sub-arc mantle. Nature 393, 777–781.

Gaetani, G.A., Grove, T.L., 1998. The influence of water on melting of mantle peridotite. Contrib. Mineral. Petrol. 131, 323–346.

Gaetani, G.A., Watson, E.B., 2000. Open system behavior of olivine-hosted melt inclusions. Earth Planet. Sci. Lett. 183, 27–41.

Grove, T.L., Bryan, W.B., 1983. Fractionation of pyroxene-phyric MORB at low pressure: an experimental study. Contrib. Mineral. Petrol. 84, 293–309.

Grove, T.L., Gerlach, D.C., Sando, T.W., 1982. Origin of cal-alkaline series lavas at Medicine Lake Volcano by fractionation, assimilation and mixing. Contrib. Mineral. Petrol. 80, 160–182.

Grove, T.L., Kinzler, R.J., Bryan, W.B., 1990. Natural and experimental phase relations of lavas from Serocki Volcano. Proc. Ocean Drill. Program: Sci. Results 106/109, 9–17.

Grove, T.L., Kinzler, R.J., Bryan, W.B., 1992. Fractionation of mid-ocean ridge basalt (MORB). In: Morgan, J.P., Blackman, D.K., Sinton, J.M. (Eds.), Mantle Flow and Melt Generation at Mid-Ocean Ridges. Geophysical Monographs. American Geophysical Union, Washington, DC, pp. 281–310.

Gudfinnsson, G.H., Presnall, D.C., 2000. Melting behavior of model lherzolite in the system $CaO-MgO-Al_2O_3-SiO_2-FeO$ at 0.7 to 2.8 GPa. J. Petrol. 41, 1241–1269.

Hildebrand, J.H., Scott, R.L., 1964. The Solubility of Nonelectrolytes. Dover, New York, NY.

Hirschmann, M.M., Baker, M.B., Stolper, E.M., 1998. The effect of alkalis on the silica content of mantle-derived melts. Geochim. Cosmochim. Acta 62, 883–902.

Jaeger, J.C., 1968. Cooling and solidification of igneous rocks. In: Hess, H.H., Poldevaart, A. (Eds.), Basalts. Wiley, New York, NY, pp. 503–536.

Johnson, K.T.M., Dick, H.J.B., Shimizu, N., 1990. Melting in the oceanic upper mantle: an ion microprobe study of diopside in abyssal peridotites. J. Geophys. Res. 95, 2661–2678.

Jurewicz, A.J.G., Watson, E.B., 1988. Cations in olivine: Part 2. Diffusion in olivine xenocrysts, with applications to petrology and mineral physics. Contrib. Mineral. Petrol. 99, 186–201.

Kelemen, P.B., Hirth, J.G., Shimizu, N., Spiegelman, M., Dick, H.J.B., 1997. A review of melt migration processes in the adiabatically upwelling mantle beneath oceanic spreading ridges. Philos. Trans. R. Soc. London 355, 283–318.

Kinzler, R.J., 1997. Melting of mantle peridotite at pressures approaching the spinel to garnet transition: application to mid-ocean ridge basalt petrogenesis. J. Geophys. Res. 102, 853–874.

Kinzler, R.J., Grove, T.L., 1992. Primary magmas of mid-ocean ridge basalts: 1. Experiments and methods. J. Geophys. Res. 97, 6885–6906.

Klein, E.M., Langmuir, C.H., 1987. Global correlations of ocean ridge basalt chemistry with axial depth and crustal thickness. J. Geophys. Res. 92, 8089–8115.

Langmuir, C.H., Hanson, G.N., 1981. Calculating mineral-melt equilibria with stoichiometry, mass balance, and single-component distribution coefficients. In: Newton, R.C., Navrotsky, A., Wood, B.J. (Eds.), Thermodynamics of Minerals and Melts. Springer-Verlag, New York, NY, pp. 247–271.

Libourel, G., 1999. Systematics of calcium partitioning between olivine and silicate melt: implications for melt structure and calcium content of magmatic olivines. Contrib. Mineral. Petrol. 136, 63–80.

Libourel, G., Boivin, P., Biggar, G.M., 1989. The univariant curve liquid = forsterite + anorthite + diopside in the system CMAS at 1 bar: solid solutions and melt structure. Contrib. Mineral. Petrol. 102, 406–421.

Marsh, B.D., 1988. Crystal size distributions (CSD) in rocks and the kinetics and dynamics of crystallization: I. Theory. Contrib. Mineral. Petrol. 99, 277–291.

Milholland, C.S., Presnall, D.C., 1998. Liquidus phase relations in the $CaO-MgO-Al_2O_3-SiO_2$ system at 3.0 GPa: the aluminous pyroxene thermal divide and high-pressure fractionation of picritic and komatiitic magmas. J. Petrol. 39, 3–27.

Misener, D.J., 1974. Cation diffusion in olivine. In: Hofman, A.W., Giletti, B.J., Yoder Jr., H.S., Yund, R.A. (Eds.), Geochemical Transport and Kinetics. Carnegie Institution of Washington, Washington, DC, pp. 117–129.

Nielsen, R.L., Michael, P.J., Sours-Page, R., 1998. Chemical and physical indicators of compromised melt inclusions. Geochim. Cosmochim. Acta 62, 831–839.

Pan, V., Longhi, J., 1990. The system $Mg_2SiO_4-Ca_2SiO_4-CaAl_2O_4-NaAlSiO_4-SiO_2$: one atmosphere liquidus equilibria of analogs of alkaline mafic lavas. Contrib. Mineral. Petrol. 105, 569–584.

Press, W.H., Flannery, B.P., Teukolsky, S.A., Vetterling, W.T., 1989. Numerical Recipes in PASCAL: The Art of Scientific Computing. Cambridge Univ. Press, New York, NY.

Qin, Z., Lu, F., Anderson Jr., A.T., 1992. Diffusive reequilibration of melt and fluid inclusions. Am. Mineral. 77, 565–576.

Saal, A.E., Hart, S.R., Shimizu, N., Hauri, E.H., Layne, G.D., 1998. Pb isotopic variability in melt inclusions from oceanic island basalts, Polynesia. Science 282, 1481–1484.

Sack, R.O., Walker, D., Carmichael, I.S.E., 1987. Experimental petrology of alkalic lavas: constraints on cotectics of multiple saturation in natural basic liquids. Contrib. Mineral. Petrol. 96, 1–23.

Schiano, P., Bourdon, B., 1999. On the preservation of mantle information in ultramafic nodules: glass inclusions within minerals versus interstitial glasses. Earth Planet. Sci. Lett. 169, 173–188.

Schiano, P., Bourdon, B., Clocchiatti, R., Massare, D., Varela, M.E., Bottinga, Y., 1998. Low-degree partial melting trends recorded in upper mantle mineral. Earth Planet. Sci. Lett. 160, 537–550.

Sewell, G., 1988. The Numerical Solution of Ordinary and Partial Differential Equations. Academic Press, New York, NY, 271 pp.

Shi, P., 1993. Low-pressure phase relationships in the system Na_2O–CaO–FeO–MgO–Al_2O_3–SiO_2 at 1100 °C, with implications for the differentiation of basaltic magmas. J. Petrol. 34, 743–762.

Shi, P., Libourel, G., 1991. The effects of FeO on the system CMAS at low pressure and implications for basalt crystallization processes. Contrib. Mineral. Petrol. 108, 129–145.

Shimizu, N., 1998. The geochemistry of olivine-hosted melt inclusions in a FAMOUS basalt ALV519-4-1. Phys. Earth Planet. Inter. 107, 183–201.

Sisson, T.W., Bronto, S., 1998. Evidence for pressure-release melting beneath magmatic arcs from basalt at Galunggung, Indonesia. Nature 391, 883–886.

Sobolev, A.V., 1996. Melt inclusions in minerals as a source of principle petrologic information. Petrology 4, 209–220.

Sobolev, A.V., Chaussidon, M., 1996. H_2O concentrations in primary melts from supra-subduction zones and mid-ocean ridges: implications for H_2O storage and recycling in the mantle. Earth Planet. Sci. Lett. 137, 45–55.

Sobolev, A.V., Danyushevsky, L.V., 1994. Petrology and geochemistry of bonitites from the north termination of the Tonga Trench: constraints on the generation conditions of primary high-Ca boninite magmas. J. Petrol. 35, 1183–1211.

Sobolev, A.V., Shimizu, N., 1993. Ultra-depleted primary melt included in an olivine from the Mid-Atlantic Ridge. Nature 363, 183–201.

Sours-Page, R., Johnson, K.T.M., Nielsen, R.L., Karsten, J.L., 1999. Local and regional variation of MORB parent magmas: evidence from melt inclusions from the Endeavor Segment of the Juan de Fuca Ridge. Contrib. Mineral. Petrol. 134, 342–363.

Tormey, D.R., Grove, T.L., Bryan, W.B., 1987. Experimental petrology of normal MORB near the Kane fracture zone, 22°–25 ° N, Mid-Atlantic Ridge. Contrib. Mineral. Petrol. 96, 121–139.

Walker, D., Shibata, T., DeLong, S.E., 1979. Abyssal tholeiites from the Oceanographer Fracture Zone: II. Phase equilibria and mixing. Contrib. Mineral. Petrol. 70, 111–125.

Walter, M.J., 1998. Melting of garnet peridotite and the origin of komatiite and depleted lithosphere. J. Petrol. 39, 29–60.

Watson, E.B., 1976. Glass inclusions as samples of early magmatic liquid: determinative method and application to a South Atlantic basalt. J. Volcanol. Geotherm. Res. 1, 73–84.

Watson, E.B., Cherniak, D.J., 1997. Oxygen diffusion in zircon. Earth Planet. Sci. Lett. 148, 527–544.

Zhang, Y., 1998. Mechanical and phase equilibria in inclusion–host systems. Earth Planet. Sci. Lett. 157, 209–222.